Duality and similarity properties of the effective permittivity of two-dimensional heterogeneous medium with inclusion of fractal geometry

Abdelilah Mejdoubi and Christian Brosseau*

Laboratoire d'Electronique et Systèmes de Télécommunications, Université de Bretagne Occidentale, CS 93837, 6 avenue Le Gorgeu, 29238 Brest Cedex 3, France

(Received 16 December 2005; revised manuscript received 8 February 2006; published 17 March 2006)

We report a systematic finite-difference time-domain study on the dielectric properties of two-dimensional lossless heterostructures with inclusion of deterministic fractal geometry (Koch's snowflake, Sierpinski's square and triangle) constrained to sit in a circumscribed circle, for a wide range of surface fractions. In all the configurations investigated, we observed (i) a strong deviation of the surface fraction dependence of the effective permittivity based on Maxwell Garnett analysis, and (ii) a permittivity change with reduced perimeter according to a similarity transformation, at least for the first three iterations of the fractal pattern. We show that the results of our numerical analysis disagree with expectations from the duality (phase interchange) relation, and explain this as being due to the intrinsic complexity of the morphology which requires a multipolar approach to correctly describe the microstructure features of these heterostructures.

DOI: 10.1103/PhysRevE.73.031405 PACS number(s): 61.43.Hv, 77.22.Ch, 41.20.Cv, 05.45.Df

I. INTRODUCTION

Understanding the dielectric properties of heterostructures has challenged both theory and experiment [1,2]. Significant progress has been made over the past two decades in understanding how to analyze the effective permittivity of composite materials with inclusion of regular and ideal geometric shapes. The archetypal examples are spherical and spheroidal inclusions in an otherwise uniform matrix [3,4]. Advanced computer hardware and computational methods have allowed some of this progress to be treated from first principles [2]. By contrast, our understanding of the fundamental properties of composite structures with the inclusion of arbitrarily complex geometry remains very limited. The challenge arises because the surface and interface between different materials involve such complexities as charge transfer, electrode polarization, polarization due to adsorbed chemical species (surface oxides and other contaminating surface layers), and Maxwell-Wagner-Sillars polarization, which will eventually affect the effective permittivity. This central issue was first posed over two decades ago [5] and a great deal of effort is now devoted to studies of the properties of complex materials, in particular, ways of forming and controlling materials of desired permittivity. In many cases of interest, the complicated irregular morphology of the inhomogeneities may be well approximated by a fractal geometry [3,6,7]. Thus, the investigation of composite materials with inclusions of fractal geometry offers an excellent platform for studying realistic models of complex materials. In addition, some insight into the dielectric behavior can be gained from symmetry considerations of the permittivity that can provide a classification scheme for complex systems. This is the focus of this work.

With the current emphasis on understanding the electromagnetic properties of three-dimensional (3D) composites, it is also of interest to consider the two-dimensional (2D) case since it has been established theoretically by Keller [8] and Dykhne [9] more than three decades ago that continuum composites with a 2D microgeometry can be characterized by a special symmetry called duality (also termed reciprocity or phase interchange relation). The generalization of this duality relation, e.g., to the case of general anisotropic permittivity tensors to any 2D two-phase composite material, disordered or not, has been given by a number of theoretical authors including Mendelson [10], Balagurov [11], Milton [12], Durand [13], and Schulgasser [14]. It is worth noting that the duality (or phase exchange) relation was first derived in terms of conductivity but for reasons of consistency we treat it, in the present work, in terms of permittivity [3,4]. It can be applied to any 2D two-phase composite as long as the x and y axes are the principal axes of the effective permittivity tensor, i.e., regardless of the phase geometry. It has been established that the effective permittivity determined in the x direction for a medium in which the inclusions (respectively, the matrix) have permittivity ε_1 (respectively, ε_2), $\varepsilon^x(\varepsilon_1,\varepsilon_2)$, is related to the effective permittivity of the phase-interchanged composite in the y direction, $\varepsilon^y(\varepsilon_2,\varepsilon_1)$, independently of the specific structure by the following equation:

$$\varepsilon^x(\varepsilon_1,\varepsilon_2)\varepsilon^y(\varepsilon_2,\varepsilon_1)=\varepsilon_1\varepsilon_2. \tag{1}$$

If the material is macroscopically isotropic, i.e., the effective permittivity tensor is rotationally invariant, then Eq. (1) reduces to $\varepsilon(\varepsilon_1,\varepsilon_2)\varepsilon(\varepsilon_2,\varepsilon_1)=\varepsilon_1\varepsilon_2$. It is widely believed that this result is independent of the details of the morphology of the material.

*Corresponding author. Also affiliated with Département de Physique, Université de Bretagne Occidentale. Email address: brosseau@univ-brest.fr

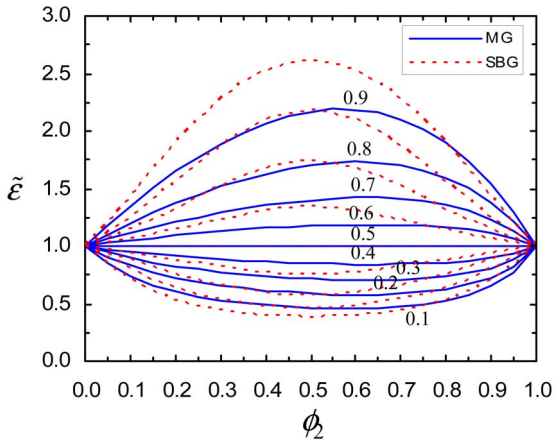

FIG. 1. (Color online) Dependence of $\tilde{\varepsilon}=\frac{\varepsilon(1,10)\varepsilon(10,1)}{10}$ as a function of ϕ_2 with the expected value from MG formula (solid line), Eq. (2a), and SBG formula (dashed line), Eq. (2b). The number denotes the value of the depolarization factor A.

In many instances the effective permittivity of a two-phase composite can be written in the generic form $\frac{\varepsilon}{\varepsilon_1}=f\left(\frac{\varepsilon_2}{\varepsilon_1},\phi_2,A\right)$, where ϕ_2 is the surface fraction of inclusion, and A $(0\leqslant A\leqslant 1)$ is the depolarization factor that depends on the shape of the inclusion. Many earlier studies have suggested interesting form for f. Two of the most prominent among all proposed forms developed for a 2D two-phase heterostructure are those of Maxwell Garnett (MG) and Bruggeman (SBG)

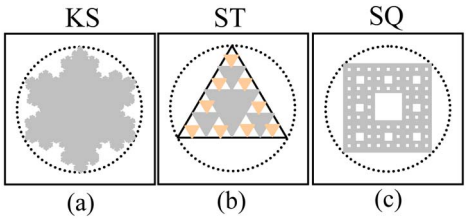

FIG. 2. (Color online) Two-dimensional structural motifs: (a) Koch's snowflake (fourth stage of iteration), (b) Sierpinski triangle (third stage of iteration), and (c) Sierpinski square (third stage of iteration). The dashed line represents the circumscribed disk containing each inclusion.

$$f\left(\frac{\varepsilon_2}{\varepsilon_1},\phi_2,A\right)=1+\frac{\phi_2\left(\frac{\varepsilon_2}{\varepsilon_1}-1\right)}{1+A(1-\phi_2)\left(\frac{\varepsilon_2}{\varepsilon_1}-1\right)}, \tag{2a}$$

and

$$f\left(\frac{\varepsilon_2}{\varepsilon_1},\phi_2,A\right)=\frac{1-A\left(1+\frac{\varepsilon_2}{\varepsilon_1}\right)+\phi_2\left(\frac{\varepsilon_2}{\varepsilon_1}-1\right)\pm\sqrt{\left[1-A\left(1+\frac{\varepsilon_2}{\varepsilon_1}\right)+\phi_2\left(\frac{\varepsilon_2}{\varepsilon_1}-1\right)\right]^2+4A(1-A)\frac{\varepsilon_2}{\varepsilon_1}}}{2(1-A)}, \tag{2b}$$

respectively. It is important to recognize that the roles of host and inclusion in the explicit form of Eq. (2a) being not reciprocal, the MG formula provides a simple example of a permittivity behavior that does not satisfy Eq. (1), except for isotropic inclusion, e.g., disk $\left(A=\frac{1}{2}\right)$. In addition it can be readily verified that, for a specific choice of the values of the permittivity of phases 1 and 2, no phase-inversion symmetry can be detected at $\phi_2=\frac{1}{2}$ (Fig. 1). In this case, duality is satisfied only if $A=\frac{1}{2}$. But, in contrast with the MG analysis, the dashed lines shown in Fig. 1 illustrate a symmetric behavior with respect to $\phi_2=\frac{1}{2}$ when the SBG form is assumed. There is a large body of work showing that Eqs. (2a) and (2b) do not accurately predict the value of ε of heterostructures outside a specific domain of system parameters [1–3]. This is mainly due to the fact that these equations do not take into account the effects of the material's microstructure on ε.

In the numerical study presented here we report on a quasistatic finite-difference time-domain (FDTD) study of two-dimensional planar composites containing a deterministic fractal inclusion. In this work, we present two major results. First, we show how the inclusion shape influences the effective permittivity of the composite material. Specifically our purpose is to illustrate that an explicit descriptor, related to a similarity transformation, can be useful to probe the dependence of the permittivity on morphology. Second, we have investigated how strongly the duality relation, Eq. (1), can be violated by composites containing fractal patterns. To the best of our knowledge, prior work has not addressed the important issue of the symmetry properties of the effective permittivity in the context of 2D heterostructures containing inclusion with fractal geometry.

The remainder of the paper is organized as follows. Our computational approach is briefly described in Sec. II. The results and discussion are presented in Sec. III. Section IV concludes our study.

II. METHODOLOGY

Three of the most thoroughly studied deterministic fractal structures are the Koch's snowflake (KS) and the Sierpinski's square (SQ) and triangle (ST) [15–17]. We have, therefore, chosen to carry out our numerical calculations on these systems. See Fig. 2 for schematic diagrams of these morphologies. For each geometry, the perimeter becomes infinitely

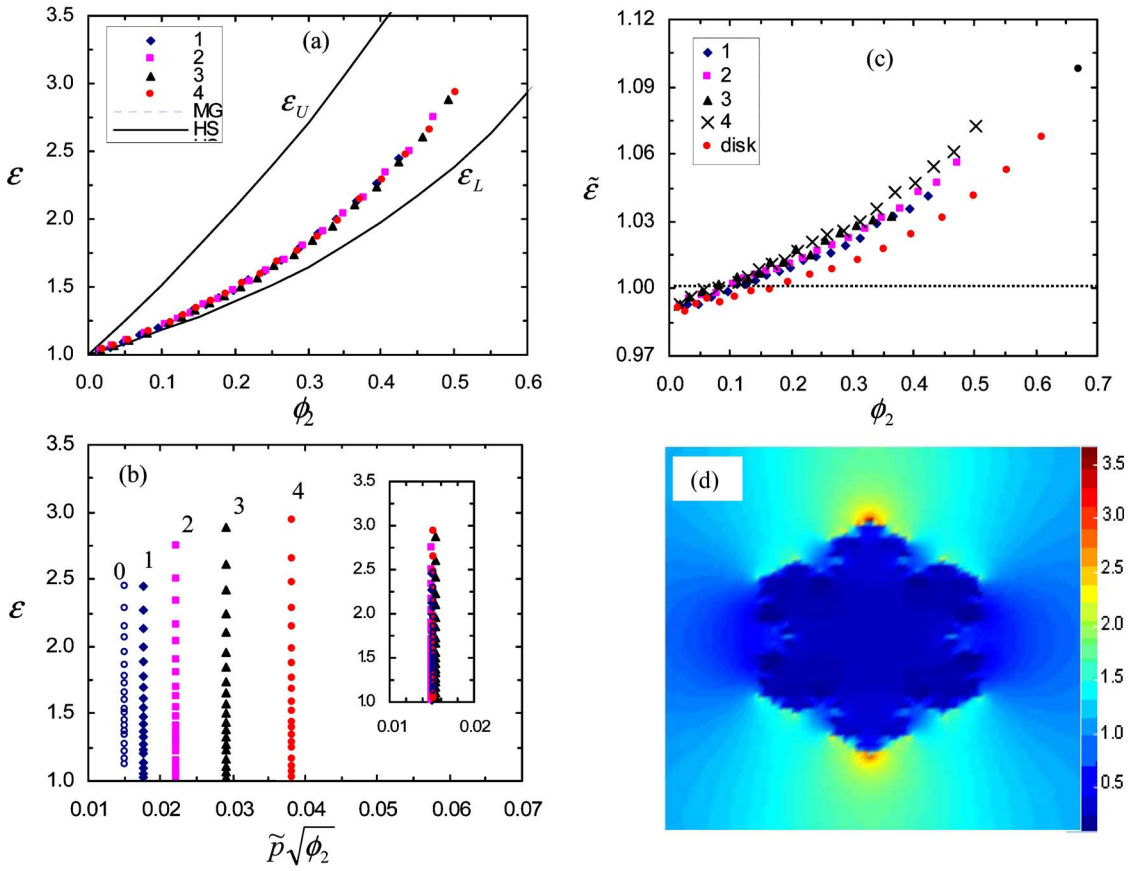

FIG. 3. (Color online) (a) A comparison of the simulated results for the effective (relative) permittivity $\varepsilon=\varepsilon^y$ of a composite containing a single inclusion with the effective medium equation of MG as a function of the surface fraction of inclusion ϕ_2. The inclusion is the KS with $\varepsilon_1=1$ and $\varepsilon_2=10$. Symbols denote the different iteration numbers n as indicated in the inset. The solid lines correspond to the permittivity evaluated by using HS upper (ε_U) and lower (ε_L) bounds, respectively. The dashed line corresponds to the MG prediction for a discoidal inclusion and cannot be distinguished from the HS lower bound. (b) Same as in (a) for the effective (relative) permittivity as a function of $\tilde{p}\sqrt{\phi_2}$. The inset shows that the similarity relations obtained by using Eq. (3) agree well with our data. The shift factors are: 0.86, 0.68, and 0.53, and 0.40 for $n=1$, 2, 3, and 4, respectively. (c) A comparison of $\tilde{\varepsilon}=\frac{\varepsilon^y(10,1)\varepsilon^x(1,10)}{10}$ as a function of ϕ_2 with the expected value, i.e., 1, from the duality, Eq. (1) relation if the material is macroscopically isotropic. For comparison we have also indicated the data corresponding to a discoidal inclusion (●). (d) Maps of the FDTD-calculated electric field vector norm $\sqrt{E_x^2+E_y^2}$. The inclusion is the third iteration of the KS with $\varepsilon_1=1$ and $\varepsilon_2=10$. The local field vector norm is normalized to the source electric field norm and is indicated by color as defined in the color bars. $\phi_2=0.18$.

large as the iteration number of the fractal pattern $\to\infty$, but for one case (KS), the surface area is bounded while for another one (SQ) the pattern is 90°-rotation invariant. Furthermore, we assume that these structures are constrained to sit in a circumscribed circle. This discoidal shape is of interest because it allows one to consider the effect of surface fraction and perimeter on the permittivity of a 2D system which has a well defined depolarization factor, in contrast to inclusion of arbitrarily complex geometry, for which A cannot be expressed in general in a closed-form expression [18].

One of the first, and still one of the most commonly used, numerical methods to simulate the electromagnetic phenomena in structures and materials is the FDTD [19]. For the computer code used to generate the results in this work, see Ref. [18]. We note at the outset that while there are several schemes to determine ε, our approach is based on the analysis of the reflection characteristics of a transmission line. Typically, the lossless two-phase composite material in the form of a slab is inserted in the cross section of a parallel-plate transmission electron microscopy (TEM) waveguide that is assumed to be infinitely long in the propagation direction of the wave (Oz). The open sides of the waveguide are modeled using a uniaxial perfectly matched layer (UPML) *ABC* [18,19] because it leads to only very small backreflections. The effective (relative) permittivity of the composite material is deduced from the knowledge of the reflection behavior at the surface of the material that is embedded in the waveguide. By using the transmission-line theory, it has been established previously the important fact that ε is related to the absolute value of the reflection coefficient R at the left side of the slab surface by

$$|R|=\frac{\left|(1-\varepsilon)\tan\left(\frac{\omega\ell}{c}\sqrt{\varepsilon}\right)\right|}{\sqrt{4\varepsilon+(1+\varepsilon)^2\tan^2\left(\frac{\omega\ell}{c}\sqrt{\varepsilon}\right)}}$$

[18,20]. In the above ℓ denotes the length of the slab and c is the speed of light. For the problem at hand, we illuminate the

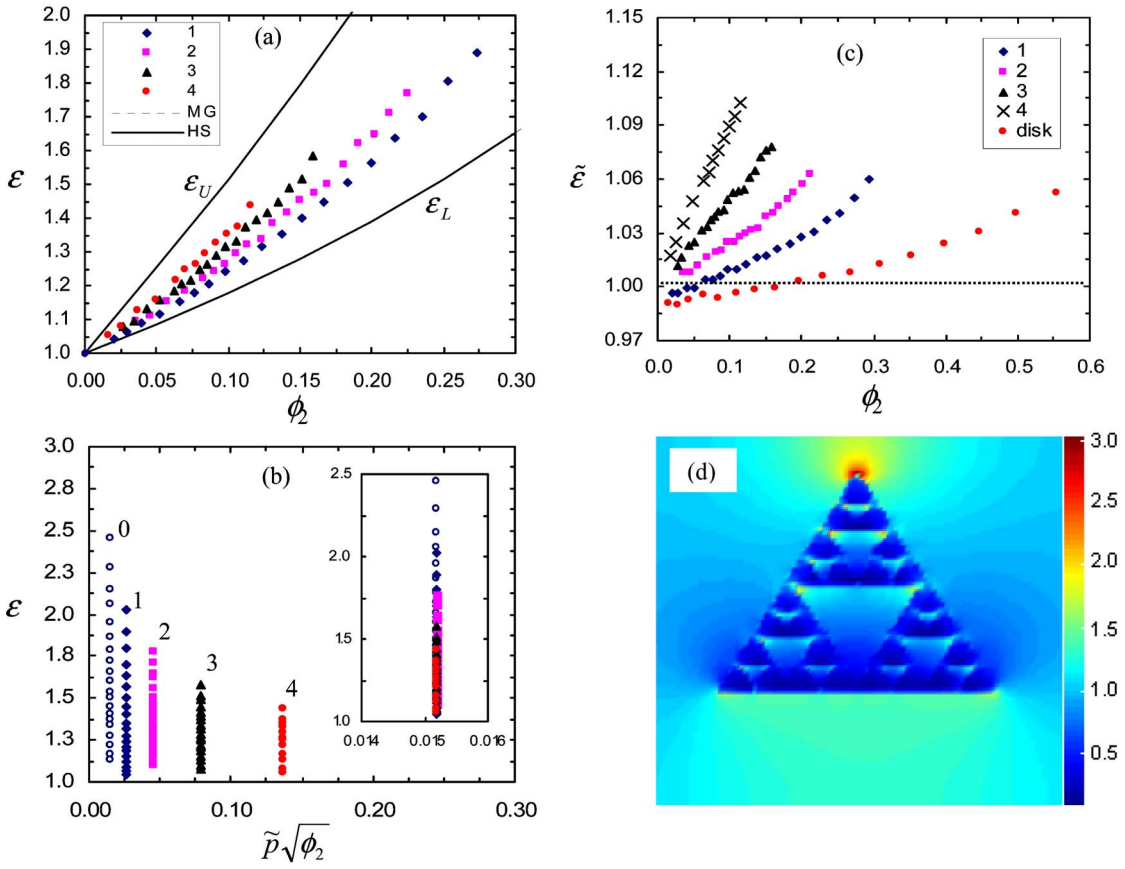

FIG. 4. (Color online) (a) A comparison of the simulated results for the effective (relative) permittivity $\varepsilon=\varepsilon^y$ of a composite containing a single inclusion with the effective medium equation of MG as a function of the surface fraction of inclusion ϕ_2. The inclusion is the ST with $\varepsilon_1=1$ and $\varepsilon_2=10$. Symbols denote the different iteration numbers n as indicated in the inset. The solid lines correspond to the permittivity evaluated by using HS upper (ε_U) and lower (ε_L) bounds, respectively. The dashed line corresponds to the MG prediction for a discoidal inclusion and cannot be distinguished from the HS lower bound. (b) Same as in (a) for the effective (relative) permittivity as a function of $\tilde{p}\sqrt{\phi_2}$. The inset shows that the similarity relations obtained by using Eq. (3) agree well with our data. The shift factors are: 0.58, 0.33, 0.19, and 0.11 for $n=1$, 2, 3, and 4, respectively. (c) A comparison of $\tilde{\varepsilon}=\frac{\varepsilon^y(10,1)\varepsilon^x(1,10)}{10}$ as a function of ϕ_2 with the expected value, i.e., 1, from the duality, Eq. (1) relation. For comparison we have also indicated the data corresponding to a discoidal inclusion (●). (d) Maps of the FDTD-calculated electric field vector norm $\sqrt{E_x^2+E_y^2}$. The inclusion is the third iteration of the ST with $\varepsilon_1=1$ and $\varepsilon_2=10$. The local field vector norm is normalized to the source electric field vector norm and is indicated by color as defined in the color bars. $\phi_2=0.10$.

slab by a simple Gaussian pulse wave. We use excitation $f=\frac{\omega}{2\pi}=10.23$ MHz well below the cutoff frequency to higher order TM (to x) modes of the parallel plate waveguide, i.e., $f_c=\frac{c}{2d}$, where d is the width of the waveguide. The FDTD calculations make use of the quasistatic approximation, and relevant aspects of the computational details are discussed in detail elsewhere [18]. This long-wavelength limit corresponds to the case that the wavelength is much larger than the system size, i.e., $\frac{\omega\ell}{c}\sqrt{\varepsilon}\ll 1$. The radius of circumscribed circle, R, containing each inclusion is under the dependence of the surface fraction of inclusion, e.g., for the third iteration of Koch's snowflake, $R=75$ mm at $\phi_2=0.18$. The length and width of the slab are set to $\ell=d=0.37$ m. The surface fraction of inclusion is denoted ϕ_2, and the reduced perimeter is $\tilde{p}=\frac{P}{K}$, where P and K are the perimeter and the surface area, respectively. For completeness, we indicate that, given the orientation of the field vector components in the waveguide, it is $\varepsilon=\varepsilon^y$ which is determined in our calculations. In practice, the calculation of ε^x requires the 90° rotation of the inclusion.

III. RESULTS AND DISCUSSION

In the following we present the results of our simulations and investigate the importance of symmetries on permittivity. We start by considering the ϕ_2 and $\tilde{p}\sqrt{\phi_2}$ dependencies of ε of composite materials with inclusion morphology illustrated in Figs. 3–5. In each figure, panel (a) compares the FDTD results and the MG prediction for a discoidal inclusion, panel (b) shows an analysis of ε in terms of a similarity transformation, panel (c) analyzes the FDTD data to see if they are consistent with the duality symmetry, and panel (d) displays a map of the electric field vector norm.

To test the predictive character of the MG formula (for a discoidal inclusion) we compare its prediction with the FDTD data summarized in Figs. 3(a), 4(a), and 5(a). The

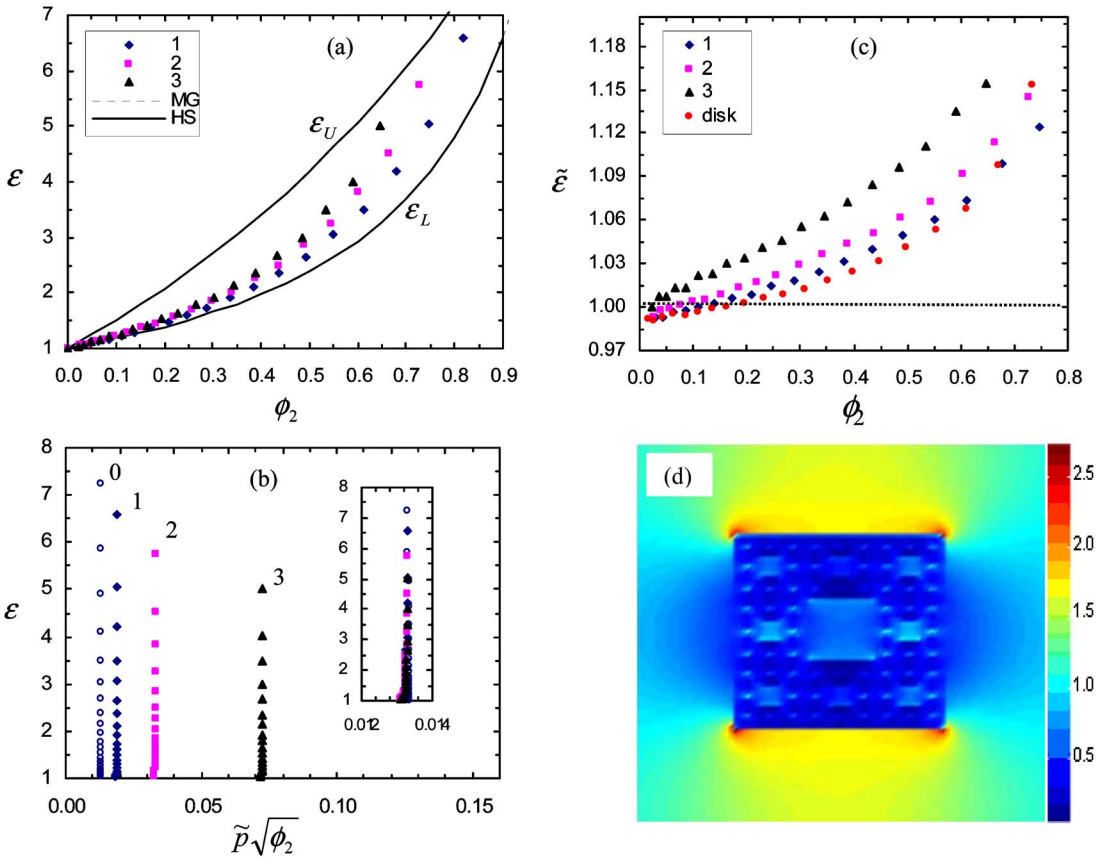

FIG. 5. (Color online) (a) A comparison of the simulated results for the effective (relative) permittivity $\varepsilon=\varepsilon^y$ of a composite containing a single inclusion with the effective medium equation of MG as a function of the surface fraction of inclusion ϕ_2. The inclusion is the KS with $\varepsilon_1=1$ and $\varepsilon_2=10$. Symbols denote the different iteration numbers n as indicated in the inset. The solid lines correspond to the permittivity evaluated by using HS upper (ε_U) and lower (ε_L) bounds, respectively. The dashed line corresponds to the MG prediction for a discoidal inclusion and cannot be distinguished from the HS lower bound. (b) Same as in (a) for the effective (relative) permittivity as a function of $\tilde{p}\sqrt{\phi_2}$. The inset shows that the similarity relations obtained by using Eq. (3) agree well with our data. The shift factors are: 0.71, 0.40, and 0.18 for $n=1$, 2, and 3, respectively. (c) A comparison of $\tilde{\varepsilon}=\frac{\varepsilon^y(10,1)\varepsilon^x(1,10)}{10}$ as a function of ϕ_2 with the expected value, i.e., 1, from the duality, Eq. (1) relation. For comparison we have also indicated the data corresponding to a discoidal inclusion (●). (d) Maps of the FDTD-calculated electric field vector norm $\sqrt{E_x^2+E_y^2}$. The inclusion is the third iteration of the SQ with $\varepsilon_1=1$ and $\varepsilon_2=10$. The local field vector norm is normalized to the source electric field vector norm and is indicated by color as defined in the color bars. $\phi_2=0.18$.

simulations reproduce the monotonic increase of ε at low surface fraction of inclusion (dilute limit), but we note that Eq. (2a) does not capture the quantitative features of the data for $\phi_2>0.15$. A similar trend is obtained if one uses Eq. (2b) instead of Eq. (2a) (not shown). In our case, this behavior is due in part to the sensitivity of the effective permittivity to the details of the morphology at a high surface fraction. In addition, we recall that MG formula is based on a dipolar description that contains no reference to microscopic features of the structure of the inclusion. These features are very similar to general observations found in the literature, e.g., Refs. [2,3,18]. It is further interesting to observe that even if one has complete information about the permittivity of each constituent and if the geometry of the composite is known, calculating ε remains difficult. Because of that difficulty, there has been much effort devoted to deriving upper and lower bounds on the allowed values of ε [3,4]. The importance and ingenuity of these methods cannot be overstated. Rigorous bounds that apply when ε_1 and ε_2 are both real and positive have been obtained using several different methods, e.g., Hashin and Shtrikman (HS) [21]. Figures 3(a), 4(a), and 5(a) display a comparison of upper and lower HS bounds on the effective permittivity and the calculated data in the present work. These graphs indicate that: (1) the MG result cannot be distinguished from the lower HS bound and (2) the FDTD prediction for the permittivity is bounded by ε_L and ε_U, but the HS bounds provide a relatively loose estimate of the actual permittivity.

Since there is a complex interplay between the surface area and perimeter effects which produces the overall features of the dielectric behavior, it is legitimate to ask what specific descriptor should be used to discriminate between the morphological features of the inclusion. Recent simulations [18] have shown that the $\tilde{p}\sqrt{\phi_2}$ dependence of ε provides us with a simple means to rationalize the dielectric behavior as the number of iteration of the fractal pattern changes. This originates from the mathematical conversion from ϕ_2 to $\tilde{p}$ which is given by $\tilde{p}_n \propto \frac{1}{d\sqrt{\phi_{2n}}}$, where n denotes

TABLE I. Relationships for geometric parameters of the topological structures considered in the present work: P, K, and d_f denote the perimeter, surface area, and Haussdorff dimension, respectively, n is the number of iteration, and R is the radius of the circumscribed disk containing each inclusion. The perimeter to surface ratio is $\tilde{p}=\frac{P}{K}$. We also define the function g as $g(n)=1+\Sigma_{k=1}^{n}4^{k-1}\left(\frac{1}{3}\right)^{2k-1}$ for $n\geq 1$, with $g(0)=1$.

Inclusion shape	Total area after the nth iteration: $R^{-2}K_n$	$R^{-2}K_\infty$	Perimeter after the nth iteration: $R^{-1}P_n$	$R^{-1}P_\infty$	Similarity ratio: $s(n)=\frac{\tilde{p}_0\sqrt{\phi_{20}}}{\tilde{p}_n\sqrt{\phi_{2n}}}$	Hausdorff dimension: d_f
KS	$\frac{3\sqrt{3}}{4}\left\{1+\frac{3}{5}\left[1-\left(\frac{4}{9}\right)^n\right]\right\}$	$\frac{6\sqrt{3}}{5}$	$3\sqrt{3}\left[\left(\frac{4}{3}\right)^n\right]$	∞	$\left(\frac{4}{3}\right)^{-n}\sqrt{g(n)}$	$d_f=\frac{\log 4}{\log 3}\approx 1.26$
ST	$\frac{3\sqrt{3}}{4}\left[\left(\frac{3}{4}\right)^n\right]$	0	$3\sqrt{3}\left[\left(\frac{3}{2}\right)^n\right]$	∞	$(3)^{-n/2}$	$d_f=\frac{\log 3}{\log 2}\approx 1.59$
SQ	$2\left[\left(\frac{8}{9}\right)^n\right]$	0	$\frac{4\sqrt{2}}{5}\left[4+\left(\frac{8}{3}\right)^n\right]$	∞	$5\left(\frac{8^{n/2}}{4(3^n)+8^n}\right)$	$d_f=\frac{\log 8}{\log 3}\approx 1.89$

the iteration number [$n=0$ corresponds to the primitive (generator) equilateral triangle for KS and ST and to the (generator) primitive square for SQ]. Furthermore, our calculations show that the relative change of $\tilde{p}\sqrt{\phi_2}$ between $n=0$ and any arbitrary value of n can be expressed as $\tilde{p}_0\sqrt{\phi_{20}}=s(n)\tilde{p}_n\sqrt{\phi_{2n}}$. Now, an essential ingredient of fractal structures is self-similarity under scale changes. These elementary considerations lead us to introduce the following relation:

$$\varepsilon_0(\tilde{p}_0\sqrt{\phi_{20}})=\varepsilon_n[s(n)(\tilde{p}_n\sqrt{\phi_{2n}})], \tag{3}$$

where ε_n is the permittivity for iteration number n. As indicated by Eq. (3), the behavior of the permittivity versus iteration number of the fractal structure can be used to obtain a single master curve. This inference is confirmed on the graph of Figs. 3(b), 4(b), and 5(b) for at least the first three iterations of the fractal patterns. To within the accuracy of our calculations a satisfactory collapse is obtained for all the data as shown in these figures.

We now turn to the effect of phase interchange on ε. The graphs displayed in Figs. 3(c), 4(c), and 5(c) show that $\tilde{\varepsilon}=\frac{\varepsilon^y(10,1)\varepsilon^x(1,10)}{10}$ is close to unity only in the dilute limit ($\phi_2<0.15$). By contrast, the simulation results for $\phi_2>0.15$ disagree with duality predictions as shown in Figs. 3(c), 4(c), and 5(c). Remarkably, we find that the enhancement of $\tilde{\varepsilon}$ relative to 1 can be substantial, i.e., $>5-10\%$ for $\phi_2=0.5$. Why does this happen? First, we recall that for a perfectly discoidal particle in the dilute limit only the dipole interaction contributes to the polarization. In the $\phi_2>0.15$ region the occurrence of structurally induced multipoles leads to other length scales and, hence, to other conditions that must be satisfied in order to physically describe the quasistatic limit of the polarization mechanisms. It is pertinent to understand the origin of the apparent conflict between the FDTD simulations of ε and the duality symmetry so ubiquitously claimed to play an important role in 2D composite materials. Since in the most basic models (MG and SBG descriptions) there is an implicit averaging whose effect is to render the composite to be both translationally and rotationally invariant, these equations are unable to describe the numerical results outside the dilute limit region. Failure of the mean-field analysis of ε can be also confirmed from Figs. 3(d), 4(d), and 5(d), which show simulation results for the local field distributions. A close look at the spatial field distributions reveals significant enhanced fields (hot spots) which are localized to the perimeter of the heterostructures. Thus, one confirms that the electric field is nonuniform inside the inclusion, thus precluding the application of effective medium theory such as that represented by the SBG equation for describing the dielectric properties of composite materials containing irregularly shaped inclusion.

The analysis presented above is relevant to any composite material that contains fractal inclusion. However, several points should be noted. (i) A basic characteristic of fractal structures is the Hausdorff dimension d_f (Table I). Typically, it is a measure of how complicated a self-similar structure is. What appears to be remarkable is that our results are in fair agreement with the similarity relation, Eq. (3), for the three structures having very different values of d_f and morphologies, i.e., the KS is connected in the sense that it does not have any breaks or gaps in it, while the ST and SQ are perforated. Because d_f for the KS is much closer to unity than for the ST and SQ as can be seen in Table I, we expect that a stronger influence of the corrugated perimeter rather than the surface area happens. This might help to explain why there are only modest differences in ε between the iterations, as seen in Fig. 3(a), when it is plotted as function of ϕ_2, whereas an ordered progression of the ε vs $\tilde{p}\sqrt{\phi_2}$ curves can be observed in Fig. 3(b). (ii) We note a limitation on our

numerical technique that prevents us from probing the similarity transformation for n is larger than n^*. When $n > n^*$, the perimeter of the inclusion in the composite material becomes very large, presumably larger than the dimension of the sample and the wavelength. Thus, we are unable to unambiguously determine the effective permittivity in the frequency range considered. To give a concrete example, it is easy to check that for the KS, the lower limit n^* is typically of the order of

$$\frac{\ln\left(\frac{c}{3\sqrt{3}Rf}\right)}{\ln\left(\frac{4}{3}\right)}$$

which is approximately equal to 10 for the largest value of ϕ_2 investigated. However, as $n \geqslant 4$ the large uncertainties in the calculated value of the perimeter may be critical for an accurate check of the similarity transformation by direct comparison with the values of $s(n)$ given in Table I. (iii) In the calculations reported here we have considered lossless composite systems, but the analysis can be easily modified to account for the absorption loss. In this case the response of the dielectric heterostructure to an oscillating electric field is expressed in terms of a complex effective permittivity $\varepsilon = \varepsilon' - j\varepsilon''$. Details will be reported in a future publication [22].

IV. CONCLUSIONS

In summary, the effective permittivity of two-dimensional two-phase lossless heterostructures with inclusion of deterministic fractal geometry has been investigated in detail via FDTD simulations. Remarkably, we found that a similarity transformation offers a direct rationalization for the permittivity as a function of the iteration number of the fractal pattern. However, there are quantitative differences between our numerical results and those expected from the duality symmetry, a subject worthy of further study. Our results confirm that the morphology dependence of permittivity in these heterostructures is governed by the concomitant changes in surface area and perimeter. However, the physics behind these empirical relations is unclear as indicated by the general lack of comparisons with experimental reports.

At the coarse grain level description of this work, we expect the results presented here to have general implications in applications ranging from dielectric characterization of pathologic biological tissues for cancer research [23], and development of artificial materials with electromagnetic response driven by surface (interface) phenomena, e.g., magneto-electric nanostructures [24]. It should be noted that, although the method developed here is a useful extension of the previous analysis that helps to account for potential influences of the inclusion shape on the dielectric properties of composite materials, two additional factors may also be important. First, our next goal is to consider random distributions of inclusions with such complex geometries and to investigate the equilibrium effective dielectric properties. This requires a statistical approach. In this context, the recent results of Refs. [25,26] for random (continuum) distributions of disks in a plane assume a particular significance. In these random materials, multiple interactions result in a litany of new behavior. Interestingly, some of these interactions can eventually compete with the surface (interface) effects described in the current paper and will produce rich dielectric properties. Second, almost all analyses to date have ignored the fact that the permittivity of each constituent in the composite is frequency dependent, i.e., dispersive material. Despite the inherent computational difficulties such calculations would be highly desirable to investigate how frequency influences the nature of the local-field enhancement around the inclusion. Finally, our study points toward the possibility of employing physics-based knowledge of dielectric heterostructures to build relevant structures for engineering applications, e.g., fractal antennas [27], or mesoporous low-permittivity materials, which will be used as interlevel dielectrics for the next generation of monolithic microwave integrated circuits [28].

ACKNOWLEDGMENT

The Laboratoire d'Electronique et Systèmes de Télécommunications is Unité Mixte de Recherche CNRS 6165.

[1] C. Brosseau, J. Phys. D (to be published).
[2] C. Brosseau and A. Beroual, Prog. Mater. Sci. **48**, 373 (2003).
[3] M. Sahimi, *Heterogeneous Materials I: Linear Transport and Optical Properties* (Springer, New York, 2003).
[4] S. Torquato, *Random Heterogeneous Materials: Microstructure and Macroscopic Properties* (Springer, New York, 2002).
[5] T. Hanai, H. Z. Zhang, K. Sekine, K. Asaka, and K. Asami, Ferroelectrics **86**, 191 (1988).
[6] B. B. Mandelbrot, *The Fractal Geometry of Nature* (Freeman, New York, 1983).
[7] K. Falconer, *Fractal Geometry: Mathematical Foundations and Applications* (Wiley, New York, 1990).
[8] J. B. Keller, J. Appl. Phys. **34**, 991 (1963); see also J. B. Keller, J. Math. Phys. **5**, 548 (1964).
[9] A. M. Dykhne, Zh. Eksp. Teor. Fiz. **59**, 110 (1970) [Sov. Phys. JETP **32**, 63 (1970)].
[10] K. S. Mendelson, J. Appl. Phys. **46**, 918 (1975); **46**, 4740 (1975).
[11] B. Ya. Balagurov, Zh. Eksp. Teor. Fiz. **81**, 665 (1981) [Sov. Phys. JETP **54**, 355 (1981)].
[12] G. W. Milton, Phys. Rev. B **38**, 11296 (1988); Phys. Rev. Lett. **46**, 542 (1981); J. Appl. Phys. **52**, 5294 (1981); in *Physics and Chemistry of Porous Media*, edited by D. L. Johnson and P. N. Sen (American Institute of Physics, New York, 1984); Commun. Math. Phys. **111**, 281 (1987).
[13] P. P. Durand and L. H. Ungar, Int. J. Numer. Methods Eng. **26**, 2487 (1988).
[14] K. A. Schulgasser, Int. Commun. Heat Mass Transfer **19**, 639

(1992).
[15] H. E. Stanley, in *Fractals and Disordered Systems*, edited by A. Bunde and S. Havlin (Springer-Verlag, Berlin, 1991).
[16] J. Feder, *Fractals* (Plenum, New York, 1988).
[17] Although the issue considered in the current work is valuable in its own right, it is also of practical importance since many pseudo-2D systems, such as colloid clusters, collapsed through deposition onto a substrate, deposited thin films, or surfaces roughened by evaporation or etching, are self-affine. See, e.g., M. Kardar, G. Parisi, and Y. C. Zhang, Phys. Rev. Lett. **56**, 889 (1986); W. M. Tong and R. S. Williams, Annu. Rev. Phys. Chem. **45**, 401 (1994); C. Douketis, Z. Wang, T. L. Haslett, and M. Moskovits, Phys. Rev. B **51**, 11022 (1995).
[18] A. Mejdoubi and C. Brosseau, J. Appl. Phys. (to be published).
[19] A. Taflove, *Computational Electrodynamics—The Finite-Difference Time-Domain Method* (Artech House Inc., Norwood MA, 1995); K. S. Yee, IEEE Trans. Antennas Propag. **AP-14**, 303 (1966); A. Taflove and S. C. Hagness, *Computational Electrodynamics: The Finite-Difference Time Domain Method*, 2nd ed. (Artech House, Boston, 2000); K. S. Kunz and R. J. Luebbers, *The FDTD Method for Electromagnetics* (CRC Press, Boca Raton, 1993).
[20] O. Pekonen, K. K. Kärkkäinen, A. H. Sihvola, and K. I. Nikoskinen, J. Electromagn. Waves Appl. **13**, 67 (1999); K. K. Kärkkäinen, A. H. Sihvola, and K. I. Nikoskinen, IEEE Trans. Geosci. Remote Sens. **GE–38**, 1303 (2000).
[21] Z. Hashin and S. Shtrikman, J. Appl. Phys. **33**, 3125 (1962). HS lower and upper bounds for any d-dimensional two-phase isotropic mixture in which $\varepsilon_2 \geqslant \varepsilon_1$ are: $\varepsilon_L = \varepsilon_1\phi_1 + \varepsilon_2\phi_2 - \frac{\phi_1\phi_2(\varepsilon_2-\varepsilon_1)^2}{\varepsilon_1\phi_2+\varepsilon_2\phi_1+(d-1)\varepsilon_1}$ and $\varepsilon_U = \varepsilon_1\phi_1 + \varepsilon_2\phi_2 - \frac{\phi_1\phi_2(\varepsilon_2-\varepsilon_1)^2}{\varepsilon_1\phi_2+\varepsilon_2\phi_1+(d-1)\varepsilon_2}$, respectively.
[22] A. Mejdoubi and C. Brosseau (unpublished).
[23] During the past decade, a large amount of experimental evidence has accumulated showing that even in biomedical sciences fractal patterns could be observed, see, e. g., G. A. Losa and T. F. Nonnenmacher, Mod. Pathol. **9**, 174 (1996).
[24] S. Mallegol, C. Brosseau, P. Queffelec, and A. M. Konn, Phys. Rev. B **68**, 174422 (2003); C. Brosseau, J. B. Youssef, P. Talbot, and A. M. Konn, J. Appl. Phys. **93**, 9243 (2003); C. Brosseau and P. Talbot, IEEE Trans. Dielectr. Electr. Insul. **11**, 819 (2004); C. Brosseau, S. Mallegol, P. Queffelec, and J. B. Youssef, Phys. Rev. B **70**, 092401 (2004).
[25] V. Myroshnychenko and C. Brosseau, Phys. Rev. E **71**, 016701 (2005).
[26] V. Myroshnychenko and C. Brosseau, J. Appl. Phys. **97**, 044101 (2005).
[27] C. Puente, J. Romeu, R. Pous, and A. Cardama, in *Fractals in Engineering*, edited by J. L. Véhel, E. Lutton, and C. Tricot (Springer, New York, 1997).
[28] These technologies will require ultralow permittivity interlevel dielectrics with effective $\varepsilon < 2.1$, which must incorporate porosity ($\varepsilon = 1$). See, e.g., *International Technology Roadmap for Semiconductors*, http://public.itrs.net/.